Real-Time, Robot-Based, 3D Localization of RFID Tags, by Transforming Phase Measurements to a Linear Optimization Problem

Anastasios Tzitzis, Andreana Malama, Vasiliki Drakaki, Aggelos Bletsas, *Senior Member, IEEE*
Traianos Yioultsis, *Member, IEEE,* Antonis G. Dimitriou, *Senior Member, IEEE*

***Abstract*—In this paper, we propose a prototype method for fast and accurate 3D localization of RFID-tagged items by a mobile robot. The robot performs Simultaneous Localization of its own pose and Mapping of the surrounding environment (SLAM). It is equipped with RFID readers and antennas placed at different heights, collecting phase-measurements by all tags. Thanks to the self-localization property of the robot, a synthetic aperture is created for each tag. In this paper, we have manipulated the set of phase-measurements, combined with the known poses of the robot to craft an overdetermined system of linear equations which pinpoints the location of the tag. The linearity of the system preserves that localization is achieved rapidly. The problem is solved for any arbitrary movement of the robot and extended in three dimensions. The proposed method is experimentally compared against the state-of-the-art in SAR-based RFID localization. It is the fastest and the most accurate, when the robot moves along straight-paths. Its accuracy slightly worsens, when the robot moves along non-straight paths, while preserving its exceptionally small running-time. It can be applied in real-time 3D localization problems, demonstrating mean 3D accuracy below 20 cm.**

***Index Terms*—RFID, Localization, Linear Optimization, SAR, Phase Unwrapping, Confidence Evaluation, Robotics, SLAM.**

I. Introduction

RFID technology has received great attention over the past years, penetrating many fields of the market, including logistics, health care, industry, military, leisure activities, etc. The advantages that make it beneficial against conventional optical technologies rest on its low cost, its high read-rate capabilities and its ability to perform without visual contact, since it exploits principles of radio frequency. A typical RFID system consists of an RFID reader, an antenna and an RFID tag, usually attached to the object of interest. A successful tag reading indicates that the tag is situated within the reading range of the reader; however, from an application perspective, this information is not always sufficient and more accurate localization is desired. Such localization is achieved by properly exploiting properties of the backscattered RFID signal measured at the reader, mainly the *i*) phase and *ii*) power (also known as "Received Signal Strength Indication" - RSSI) of the tag's backscattered signal. In such framework, various localization systems and algorithms have been developed to perform localization in two (2D) and three dimensions (3D).

Exploiting the signal's power to locate a tag, usually refers to the usage of a propagation model that estimates the antenna-to-tag distance [1] - [3]. However, modeling the propagation environment in an accurate way is quite challenging, while the information of RSSI is pretty sensitive to the tag's orientation, its attachment to different materials and multipath effects. From this perspective, phase represents a more reliable information, thanks to its tolerance on the tag's orientation, but it is challenged by the 2π periodicity. Due to this periodicity, a single value of phase cannot reflect the true antenna-to-tag distance, hence multiple phase measurements are required.

Angle-of-Arrival (AoA) techniques [4]- [7] employ a pair of antennas and calculate the difference of the recorded phase to estimate the direction of the tag. When estimates by additional pairs of antennas are combined, the exact position of the tag in the 2D plane can be estimated via triangulation. Similarly, [8] calculates the phase differences between two sufficiently close antennas to define a two-dimensional hyperbolic locus, where the tag may be located at. Additional antenna-pairs introduce more hyperbolas, the intersection of which represents the tag's location. The accuracy of such methods strictly depends on the number of antennas employed in the area of interest. However, an inventory solution based on a fixed installation of multiple antennas and readers has great cost, demands maintenance and cannot adapt to changes in the environment.

Alternatively, Synthetic Aperture (SAR) systems exploit mobility of the reader to collect measurements by a single antenna at multiple locations. The SAR-based approach was first applied for radar imaging [9] and adjusted to RFID technology in [10]. Phase measurements obtained along a single-antenna synthetic aperture are fused to construct a holographic image, which essentially represents the probability of each image-point to be the actual tag's location. The solution of the problem is sought exhaustively over a grid assigned to the space of interest. In such framework, [11] - [13] present the deployment of inverse synthetic apertures that are generated by moving tags and static antennas in order to track the trajectory of a tag. Localization solutions that employ moving antennas should be accompanied by a handling system that controls and moves the antenna. Such systems are mostly operated

Manuscript received June 28, 2021
This research has been co-financed by the European Union and Greek national funds through the Operational Program Competitiveness, Entrepreneurship and Innovation, under the call RESEARCH – CREATE – INNOVATE (project code:T2EDK-02000).

Aggelos Bletas is with the Dept. of Electrical and Computer Engineering, Technical University of Crete, Greece, e-mail: aggelos@telecom.tuc.gr.
All other authors are with the School of Electrical and Computer Engineering, Aristotle University of Thessaloniki, Greece, e-mail: antodimi@auth.gr.

manually and require human intervention and effort. Moreover, some sort of information about the antenna's locations over time is a prerequisite for SAR-based methods, necessitating a time-consuming manual measuring process.

On the contrary, RFID-augmented robots capable of navigating autonomously to the vicinity of the tags and localizing themselves inside the environment, can free the localization process from human effort. [14] - [23] mount an RFID reader and antenna on a robotic vehicle. In [14] - [16], tag's location is estimated in 2D, similarly to holographic imaging, by deploying the Maximum Likelihood Estimation (MLE) approach, according to which the tag's location coincides with the solution of a matching function. Due to the non-convexity of the latter, the solution is identified by performing exhaustive search over a grid of possible tag locations. The computational burden of such techniques is proportional to the size of grid-points and can be huge for large search spaces. The antenna positions in [14] are made available by a camera system installed on the ceiling, while [16] - [17] estimate the robot's trajectory by means of a Kalman-based algorithms which fuse measurements of a few reference RFID tags with odometry data.

[18] tackles the problem of the time-consuming search over a grid, by performing phase unwrapping to the collected measurements and exploiting an unwrapped phase-distance model. This preserves convexity of the crafted matching function, which is rapidly solved by standard non linear optimization algorithms, an effect that supports the real-time application of the method. In addition to RFID equipment, the robotic vehicle employed in [18] carries laser and cameras to perform Simultaneous Localization And Mapping (SLAM). The robot can enter an unknown area, create a 2D/3D map of the environment and constantly track itself inside it. [19] also employs a SLAM-enabled mobile robot, while RFID localization is performed by phase-based particle filtering.

As for localization in 3D space, measurements by at least two antennas is often a prerequisite, while the expected localization error decreases as the number of antennas increases. [24] - [25] install a minimum of 4 antennas to record the power of the tag's signal and estimate the antenna-to-tag distances computed. Instead of installing multiple antennas, a single antenna that moves along two perpendicular directions is also able to perform 3D localization, [26] - [27]. [20] deploys a robotic vehicle that moves along a corridor to collect measurements by a single antenna. It is proven, both theoretically and experimentally, that any non straight trajectory of the robot is able to solve the 3D problem by a single antenna, while the localization problem is rapidly solved by convex optimization. A numerical analysis investigates the correlation of the robot trajectory's curvature with the reliability and accuracy of the tag estimations. The efficiency of single-antenna solution is poor when the trajectory is not sufficiently curved, an effect that raises the necessity of employing at least two antennas on the robot, such that the localization performance is independent of the robot's path.

[21] processes phase measurements collected by multiple antennas mounted on a robot to construct a multi-variable least square problem. Phase unwrapping preserves the convex-type property of the objective function, which is minimized by non linear optimization. A proposed reliability metric based on the curvature of the objective function, in combination with the high execution speed of the algorithm, allows the problem to be solved by considering measurements originated by all possible combinations of antennas, while the most reliable estimation represents the solution of the problem. [22] exploits phase measurements collected by tmultiple antennas mounted on a robotic vehicle and seeks the point of a grid that corresponds to the global solution of a matching function. Due to the existence of multiple local minima and maxima, the solution is identified by a computationally expensive grid-search, while [23] improves the algorithm's execution speed by performing particle swarm optimization on the search space. Finally, the system proposed in [28] consists of multiple transmitter and receiver antennas and it seeks the problem's solution by means of particle filtering.

In this paper, a prototype localization SAR method is proposed, capable of solving both the two-dimensional and three-dimensional localization problem. It employs multiple antennas attached on a SLAM-enabled robotic base and by exploiting differences of phase measurements and spatial properties of the problem's geometry, it crafts a linear least square problem, which essentially estimates the bearing and the range of the tag on the antenna's horizontal plane. Thanks to the linear nature of the system, it can be rapidly solved by simple matrix operations, an effect that supports the algorithm's real-time application. The proposed technique is developed for both straight and non straight trajectories. Additionally, a metric has been introduced to quantify the reliability of the estimation based, among others, on the "quality" of the available measurements. Finally, the proposed method is extended in 3D space, where data from multiple antennas, located at different heights on top of the robot, are available. The linear least square problem calculates a circular locus around each antenna's aperture. The 3D location of the tag is identified as the point in space that minimizes the sum of its distances from all loci.

A numerical analysis and an excessive experimental campaign evaluate the performance of the proposed method with respect to accuracy and running-time, achieving 3D localization error comparable to state-of-the-art and improved running time. The experiments were conducted by a SLAM-enabled robot, which is able to enter any unknown area, create a map of the environment by fusing odometry, laser and camera data, while it continuously estimates its own pose inside the map as it navigates to the vicinity of the tags.

Section II addresses the characteristics and challenges of the signal's phase. The proposed two-dimensional localization scheme that exploits a single antenna and the three-dimensional scheme that exploits multiple antennas, are presented in sections III and section IV, respectively. Section V evaluates the system's 2D performance by conducting a numerical analysis, while the experimental results and comparisons are presented in VI. Finally, section VII concludes our findings.

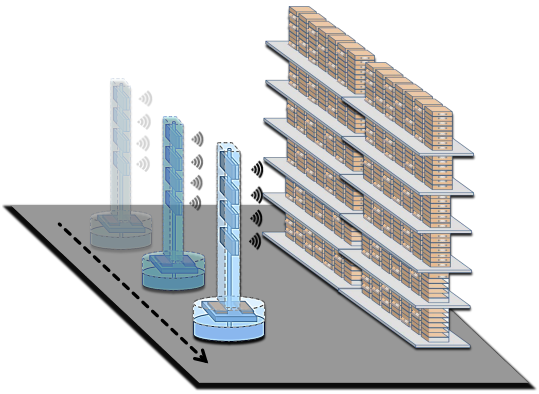

Fig. 1: An inventorying scenario where a RFID-equipped robot localizes the surrounding RFID-tagged objects.

II. Background

Fig. 1 depicts a typical indoor scenario, where a robot equipped with RFID reader(s) and antenna(s) navigates in a warehouse's corridor and inquires the surrounding RFID tags. The antennas are directional and laterally mounted on the robot, thus illuminating a specific half-space as the robot moves.

A static RFID tag placed at $\boldsymbol{A}_{tag} = [x_{tag}, y_{tag}, z_{tag}]$ is read N times by the moving antenna, leading to the generation of a synthetic aperture, Fig. 2 (a). Each reading refers to the measurement of the backscatterred signal's phase, denoted as $\phi_n^{meas},\ n \in [1, N]$. Phase is accompanied by knowledge of the antenna's pose, which consists of the coordinates of the antenna $\boldsymbol{A}_n = [x_n, y_n, z_n],\ n \in [1, N]$, the direction of motion represented by unit vector $\overrightarrow{u_n},\ n \in [1, N]$ and the direction of of the main lobe of its radiation pattern represented by unit vector $\overrightarrow{v_n},\ n \in [1, N]$; for now on, this direction will be referred to as direction of radiation. Since the antenna is mounted laterally on the robot, the direction of radiation is always perpendicular to the moving direction, namely $\overrightarrow{v_n} \perp \overrightarrow{u_n},\ \forall n \in [1, N]$. The Euclidean distance between antenna and tag is d_n:

$$d_n = \|\boldsymbol{A}_{tag} - \boldsymbol{A}_n\|_2, \quad n \in [1, N]. \tag{1}$$

Fig. 2 (b) shows the phase profile measured by an antenna that moves along the trajectory of Fig. 2 (a):

- A $\rightarrow$ B: Phase decreases, as the antenna-to-tag distance decreases; when phase decreases to the value of 0, a discontinuity occurs and phase "jumps" to the value of 2π.
- B: The phase profile exhibits a change of the slope's sign (local minimum) that corresponds to the minimum antenna-to-tag distance, i.e. the antenna is perpendicular opposite to the tag; phase stops decreasing and starts increasing.
- B $\rightarrow$ C: Phase increases, as the antenna-to-tag distance increases; a discontinuity occurs when phase increases to the value of 2π and it drops to the value of 0.

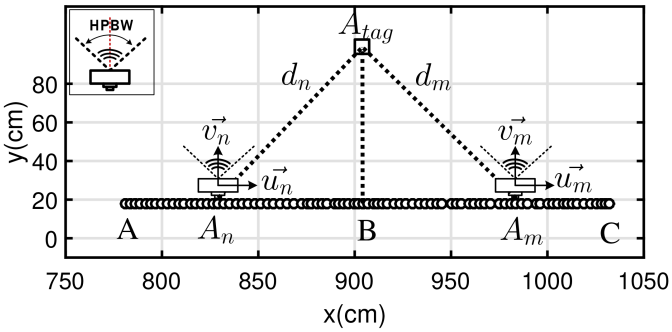

(a) The synthetic aperture generated by a single antenna moving along a straight path.

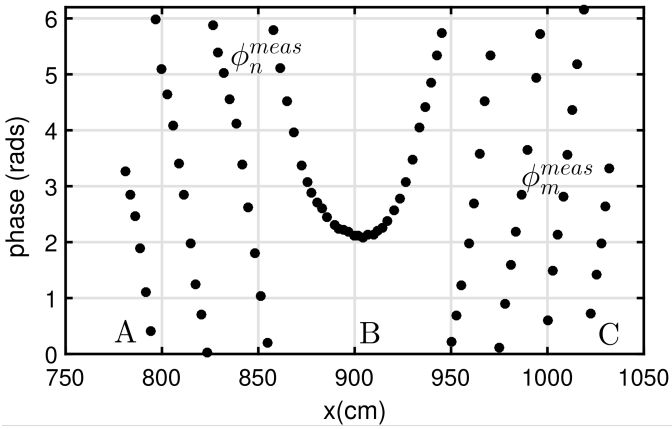

(b) The measured phase profile.

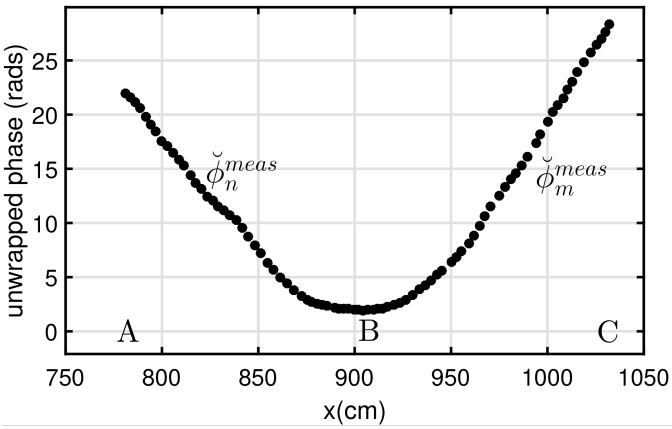

(c) The unwrapped phase profile.

Fig. 2: Visualization of the single-antenna synthetic aperture and the collected set of phase samples.

The expected phase ϕ_n^{exp} that would have been measured in Line-of-Sight (LOS) conditions for given locations of antenna and tag, is a function of their distance d_n:

$$\phi_n^{exp}(d_n) = \left(\frac{2\pi}{\lambda} 2d_n + \phi_0\right) \bmod 2\pi, \quad n \in [1, N]. \tag{2}$$

In (2), the first term of the summation corresponds to phase rotation over the travelled distance of the signal; λ stands for the wavelength of the carrier frequency, while $2d_n$ accounts for forth and back propagation since in backscatter communication, the signal travels a total distance of two times the

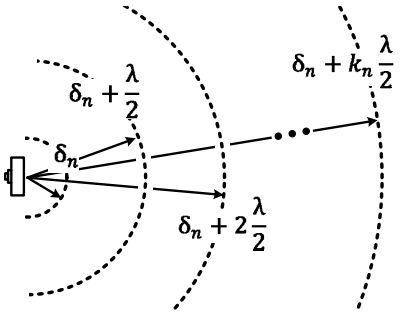

Fig. 3: Distance ambiguity imposed by the 2π periodicity of phase: a single phase measurement reflects a series of distance values $\delta_n + k_n \frac{\lambda}{2}$

antenna-to-tag distance. The second term, ϕ_0, is an additional phase rotation, independent of wave propagation. The tag's circuits, the electronics of the reader's transmitter and receiver, the antenna's cables, etc, introduce a further shifting to the measured phase, which should be accounted in (2). For the same antenna-tag pair though, this offset is common for all N phase measurements.

The modulo 2π operation is introduced so that the expected phase takes values in 2π intervals, in accordance to the measured phase. Due to this operation, any distance value with

$$d_n = \delta_n + k_n \frac{\lambda}{2}, \quad n \in [1, N] \tag{3}$$

outputs same expected phase in (2). This property raises an ambiguity; phase cannot directly reflect the true value of antenna-to-tag distance d_n, but a series of possible values which differ from each other by k_n increments of half wavelengths. $k_n \in \mathbb{Z}$ represents essentially an ambiguity term and in general is not common for all measurements. Fig. 3 visualizes this issue.

Since the unknown phase rotation ϕ_0 is considered common for all measurements of same antenna-tag pair, it can be cancelled out by exploiting the difference between any two distance values d_n and d_m with $n, m \in [1, N]$, such that

$$\Delta d_{nm} = \frac{\lambda}{4\pi} \Delta\phi_{nm}^{meas} + \Delta k_{nm} \frac{\lambda}{2}, \quad n, m \in [1, N] \tag{4}$$

where $\Delta\phi_{nm}^{meas} = \phi_n^{meas} - \phi_m^{meas}$ and $\Delta k_{nm} = k_n - k_m$. On the contrary, the unknown variables k_n and k_m may not be equal and thus, Δk_{nm} in (4) is nonzero and should be treated accordingly.

This effect can be tackled by performing phase unwrapping; i.e. the reconstruction of the original phase profile such that the 2π jumps and drops are eliminated. By properly adding multiples of 2π to each measured sample ϕ_n^{meas}, a continuous phase curve is formed, free of discontinuities. The unwrapped phase sample is denoted as $\breve{\phi}_n^{meas}$. Fig. 2 (c) depicts the unwrapped phase profile, which in contrast to the original one, has support in $(-\infty, +\infty)$.

- A $\rightarrow$ B: Phase decreases monotonously, as the antenna-to-tag distance decreases.
- B: The global minimum of the unwrapped phase profile corresponds to the minimum antenna-to-tag distance.
- B $\rightarrow$ C: Phase increases monotonously, as the antenna-to-tag distance increases.

The unwrapped phase model is modulo-free:

$$\breve{\phi}_n^{exp}(d_n) = \frac{2\pi}{\lambda} 2d_n + \phi_0, \quad n \in [1, N]. \tag{5}$$

Thanks to phase unwrapping and the removal of the modulo operation, the distance ambiguity is now common for all samples, namely $k_n = k, \ \forall \ n \in [1, N]$ in (3) and $\Delta k_{nm} = 0 \ \forall \ n, m \in [1, N]$ in (4). The distance difference Δd_{nm} is now given by:

$$\Delta d_{nm} = \frac{\lambda}{4\pi} \Delta\breve{\phi}_{nm}^{meas}, \quad n, m \in [1, N] \tag{6}$$

where $\Delta\breve{\phi}_{nm}^{meas} = \breve{\phi}_n^{meas} - \breve{\phi}_m^{meas}$ refers to the unwrapped phase.

III. Two-dimensional Localization by Single-Antenna Aperture

The method proposed in this section deals with the problem of localizing a static tag in 2D space, i.e. one coordinate of the tag's location is considered known. More specifically, by exploiting phase differences and properties of the problem's geometry, one can estimate the range and bearing of the tag with respect to the antenna. The problem is solved on the horizontal plane defined by the antenna's height; i.e. the tag is assumed to be placed at the same height as the antenna. The proposed method is called "PD-Loc" after Phase Difference-based Localization and requires small modifications depending on the type of the synthetic aperture (the robot's trajectory).

A. Straight Synthetic Aperture

Fig. 4 shows the geometry of a straight synthetic aperture in x-y plane. The symbols depicted in Fig. 4 are addressed as following:

- $\boldsymbol{A}_{tag}$: the unknown tag's location.
- $\boldsymbol{A}_n, \ n \in [1, N]$: the antenna location that corresponds to the n^{th} phase measurement ϕ_n^{meas}.
- $\overrightarrow{u_n}, \ n \in [1, N]$: the unit vector that represents the direction of antenna's movement at location $\boldsymbol{A}_n$. Since the antenna is moving towards a straight line, the direction of motion remains unchanged, $\overrightarrow{u_n} = \overrightarrow{u}, \ \forall n \in [1, N]$.
- $\overrightarrow{v_n}$: the unit vector that represents the direction of antenna's radiation at location $\boldsymbol{A}_n$. Since the antenna is moving towards a straight line, the direction of radiation remains unchanged, $\overrightarrow{v_n} = \overrightarrow{v}, \ \forall n \in [1, N]$.
- $\overrightarrow{e_x}, \overrightarrow{e_y}, \overrightarrow{e_z}$: the unit vectors along x, y and z axis, respectively; they form a set of mutually orthogonal vectors. Since vectors $\overrightarrow{u}$ and $\overrightarrow{v}$ lay on the x-y plane, $\overrightarrow{u}$, $\overrightarrow{v}$ and $\overrightarrow{e_z}$ also form a set of mutually orthogonal vectors, $\overrightarrow{v} = \overrightarrow{e_z} \times \overrightarrow{u}$.
- $d_n, \ n \in [1, N]$: the distance between the tag and the n^{th} antenna location, $d_n = \|\boldsymbol{A}_{tag} - \boldsymbol{A}_n\|_2$.
- $\boldsymbol{A}_R$: a location among $\{\boldsymbol{A}_1, \cdots, \boldsymbol{A}_N\}$ that will be used as reference point to generate distance differences. Contextually, the phase measured at $\boldsymbol{A}_R$ is denoted as ϕ_R^{meas}.
- d_R: the distance between the tag and the reference location, $d_R = \|\boldsymbol{A}_{tag} - \boldsymbol{A}_R\|_2$.

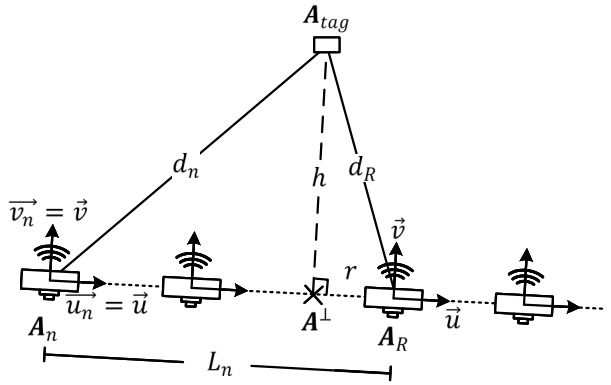

Fig. 4: Geometry of a straight synthetic aperture shown in plan view.

- $L_n,\ n \in [1, N] - \{R\}$: the known distance between the reference and the n^{th} antenna location, $L_n = \|\boldsymbol{A}_R - \boldsymbol{A}_n\|_2$.
- $\boldsymbol{A}^{\perp}$: the point on the direction of antenna's motion, which has the minimum distance from the tag. The line that joins the tag with $\boldsymbol{A}^{\perp}$ is perpendicular to the antenna's path-line. As a result, that line is considered parallel to the direction of radiation $\overrightarrow{\boldsymbol{A}^{\perp}\boldsymbol{A}_{tag}} \parallel \overrightarrow{v}$.
- r: the distance between the reference point and the closest-to-tag point, $r = \|\boldsymbol{A}_R - \boldsymbol{A}^{\perp}\|_2$.
- h: the shortest distance between the tag and the antenna's path-line, $h = \|\boldsymbol{A}_{tag} - \boldsymbol{A}^{\perp}\|_2$.

According to the above scheme, the unknown tag's position $\boldsymbol{A}_{tag}$ is given by:

$$\boldsymbol{A}_{tag}^{2D} = \underbrace{\boldsymbol{A}_R + r\overrightarrow{u}}_{\boldsymbol{A}^{\perp}} + h\overrightarrow{v} \tag{7}$$

Thus, the method's target should be the estimation of quantities r and h. The distance between the reference location and the tag is given by:

$$d_R = \sqrt{r^2 + h^2}, \tag{a}$$

while the distance between the $n^{th},\ n \in [1, N] - \{R\}$ antenna location and the tag is given by:

$$d_n = \sqrt{(r \pm L_n)^2 + h^2}. \tag{b}$$

For the $n^{th},\ n \in [1, N] - \{R\}$ antenna location, the difference between the aforementioned distances is defined as:

$$\begin{aligned} \Delta d_n = d_R - d_n \Rightarrow \\ \Delta d_n = \sqrt{r^2 + h^2} - \sqrt{(r \pm L_n)^2 + h^2}. \end{aligned} \tag{c}$$

By raising (c) to the square, the latter becomes

$$\begin{aligned} \Delta d_n^2 = r^2 + h^2 - 2\sqrt{r^2 + h^2}\sqrt{(r \pm L_n)^2 + h^2} + \\ +(r \pm L_n)^2 + h^2. \end{aligned} \tag{d}$$

By substituting term $\sqrt{(r \pm L_n)^2 + h^2}$ from (c) again in (d):

$$\begin{aligned} \Delta d_n^2 = r^2 + h^2 - 2\sqrt{r^2 + h^2}(\sqrt{r^2 + h^2} - \Delta d_n) + \\ +(r \pm L_n)^2 + h^2 \Rightarrow \\ \Delta d_n^2 = 2\sqrt{r^2 + h^2}\Delta d_n \pm 2rL_n + L_n^2. \end{aligned} \tag{e}$$

After substituting (a) in (e):

$$\Delta d_n^2 - L_n^2 = 2\Delta d_n d_R \pm 2L_n r. \tag{f}$$

Notice that we have managed to exclude the square-terms r^2, h^2 from (f), thus creating a linear system of equations, with respect to unknowns d_R, r. By substituting (6) in (f), an algebraic relation is formed, which associates the unknown quantities d_R and r with the measured phase difference:

$$\left(\frac{\lambda}{4\pi}\Delta\breve{\phi}_n^{meas}\right)^2 - L_n^2 = 2\left(\frac{\lambda}{4\pi}\Delta\breve{\phi}_n^{meas}\right)d_R \pm 2L_n r, \tag{8}$$

where $\Delta\breve{\phi}_n^{meas} = \breve{\phi}_R^{meas} - \breve{\phi}_n^{meas}$ is the difference between the unwrapped phase recorded at the reference location $\breve{\phi}_R^{meas}$ and the $n^{th},\ n \in [1, N] - \{R\}$ unwrapped phase measurement $\breve{\phi}_n^{meas}$. Again, it is reminded that distances L_n are known from the localization-algorithm of the robot. Thanks to the substitution taken place in (d), the resulted equation (8) is **linear** in its unknown coefficients d_R and r. Based on (8), a linear system can be constructed, whose matrix form is given by:

$$\begin{aligned} \boldsymbol{A}\boldsymbol{x} = \boldsymbol{b}, \\ \boldsymbol{A} = 2\begin{bmatrix} \frac{\lambda}{4\pi}\Delta\breve{\phi}_1^{meas} & \pm L_1 \\ \frac{\lambda}{4\pi}\Delta\breve{\phi}_2^{meas} & \pm L_2 \\ \vdots & \vdots \\ \frac{\lambda}{4\pi}\Delta\breve{\phi}_{N-1}^{meas} & \pm L_{N-1} \end{bmatrix} \boldsymbol{x} = \begin{bmatrix} d_R \\ r \end{bmatrix} \\ \boldsymbol{b} = \begin{bmatrix} \left(\frac{\lambda}{4\pi}\Delta\breve{\phi}_1^{meas}\right)^2 - (L_1)^2 \\ \left(\frac{\lambda}{4\pi}\Delta\breve{\phi}_2^{meas}\right)^2 - (L_2)^2 \\ \vdots \\ \left(\frac{\lambda}{4\pi}\Delta\breve{\phi}_{N-1}^{meas}\right)^2 - (L_{N-1})^2 \end{bmatrix} \end{aligned} \tag{9}$$

System (9) consists of $N-1$ equations and two unknown parameters. Since it is an overdetermined system, the solution $\boldsymbol{x} = [d_R,\ r]^T$ is computed in a least square sense, such that:

$$\boldsymbol{x} = \arg\min_{\boldsymbol{x}} \|\boldsymbol{A}\boldsymbol{x} - \boldsymbol{b}\|_2^2 = (\boldsymbol{A}^T\boldsymbol{A})^{-1}\boldsymbol{A}^T\boldsymbol{b}. \tag{10}$$

As soon as d_R and r are available, h can be computed by (a) and eventually the tag's location by (7).

Equation (7) solves the 2D localization problem on the antenna's horizontal plane. The 3D interpretation of the solution though, is a circle in the plane defined by unit vectors $\overrightarrow{v}$ and $\overrightarrow{e_z}$ (with $\overrightarrow{u}$ being its normal vector), with center $\boldsymbol{A}^{\perp}$ and radius h, see Fig. 5. The parametric equations of the above circle are:

$$\begin{cases} x = A_x^{\perp} + h\cos(\theta)v_x \\ y = A_y^{\perp} + h\cos(\theta)v_y \\ z = A_z^{\perp} + h\sin(\theta) \end{cases} \tag{11}$$

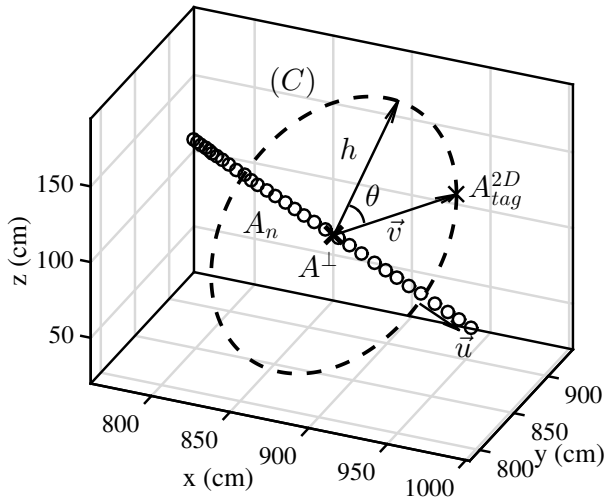

Fig. 5: The 3D locus of possible tag locations corresponding to a straight synthetic aperture.

where $A_x^{\perp}$, $A_y^{\perp}$, $A_z^{\perp}$ are the x, y, z coordinates of the circle's center $\boldsymbol{A}^{\perp}$ respectively, v_x and v_y are the x and y components of unit vector $\overrightarrow{v}$, respectively and θ goes from 0 to π. Assuming that one of the tag coordinates is known, the remaining two can be easily derived by (11).

1) Reference Selection: In case of straight aperture, the functionality of the method does not depend on the selection of reference location $\boldsymbol{A}_R$ and any antenna location $\boldsymbol{A}_n,\ n \in [1, N]$ can be employed as reference. However, the reference phase sample $\breve{\phi}_R^{meas}$ that is used to form the phase differences $\Delta\breve{\phi}_n^{meas},\ n \in [1, N] - \{R\}$ is involved in all equations of system (9) and hence, it contributes quite significantly to the calculation of the system's solution. Therefore, $\breve{\phi}_R^{meas}$ should be a measurement as accurate as possible. Such measurement would be the minimum of the unwrapped phase profile, since it represents the minimum antenna-to-tag distance and the LOS link is expected to have a strong contribution, whilst the multipath contribution should be weak. Taking into account the above, the antenna location that records the minimun phase is chosen as reference point $\boldsymbol{A}_R$.

2) Evaluation of the solution: The performance of the localization depends mainly on the number and quality of measurements. Inadequate collection of measurements would lead to a poor estimation, while noise/multipath corrupted measurements are expected to deteriorate the method's accuracy. This effect will be reflected in the variance/standard deviation of the estimated parameters $\boldsymbol{x}$; i.e. a statistical measurement that quantifies the (un)reliability of the computed solution based on the quality of data. Small values of variance/standard deviation indicate that the estimated solution is highly likely to be quite close to the actual one, whilst larger variance values imply that the estimation can significantly differ from the actual solution. Thus, the smaller the variance, the greater the confidence of the estimation.

Once the problem's parameters are estimated, their variance should be computed in order to obtain an intuition of their reliability and expected error. The variance of each parameter in $\boldsymbol{x} = [d_R, r]^T$ is given by the respective diagonal element of the covariance matrix:

$$\sigma_{d_R}^2 = C(1,1) \tag{12}$$

$$\sigma_r^2 = C(2,2). \tag{13}$$

$\boldsymbol{C}$ is a 2×2 matrix computed for linear problems by:

$$\boldsymbol{C} = (\boldsymbol{A}^T\boldsymbol{A})^{-1}\boldsymbol{\sigma}_r^2 \tag{14}$$

with $\boldsymbol{\sigma}_r^2$ being the residuals' variance. Eventually, the variances are exploited to derive the accumulated standard deviation of the tag's estimation, defined as:

$$\sigma_{est} = \sqrt{\sigma_{d_R}^2 + \sigma_r^2}. \tag{15}$$

B. Non Straight Synthetic Aperture

The robot is expected to move across corridor-type environments, which mostly require straight movements. Section III-A presented the implementation of PD-Loc applied to measurements collected along straight synthetic apertures. However, there are cases where non straight robot paths would be employed; e.g. a robot avoiding an obstacle along a corridor. The complicated geometry of a non straight problem necessitates some modifications to be made in order to craft a system able to be solved similarly to Section III-A. In the straight case, by computing parameter r, the point with the minimum distance from the tag $\boldsymbol{A}^{\perp}$ can be estimated on the direction of the antenna's motion. On the contrary, such computation is not feasible in non straight trajectories, since the direction of motion does not remain stable. The problem is treated under the assumption that the point with minimum distance from the tag $\boldsymbol{A}^{\perp}$ is the antenna location at which the minimum unwrapped phase was recorded. This location is also used as reference $\boldsymbol{A}_R$, as will be demonstrated below. Eventually, a solvable system is formed, which consists of only one parameter.

Fig. 6 depicts the geometry of a non straight synthetic aperture in plan view. The symbols of Fig. 6 are addressed as following:

- $\boldsymbol{A}_{tag}$: the unknown tag's location.
- $\boldsymbol{A}_n,\ n \in [1, N]$: the antenna location that corresponds to the n^{th} phase measurement ϕ_n^{meas}.
- $\overrightarrow{u_n},\ n \in [1, N]$: the unit vector that represents the direction of antenna's movement at location $\boldsymbol{A}_n$.
- $\overrightarrow{v_n}$: the unit vector that represents the direction of antenna's radiation at location $\boldsymbol{A}_n$.
- $\overrightarrow{e_x}, \overrightarrow{e_y}, \overrightarrow{e_z}$: the unit vectors along x, y and z axis, respectively; they form a set of mutually orthogonal vectors. Since vectors $\overrightarrow{u_n}$ and $\overrightarrow{v_n}$ lay on the x-y plane, $\overrightarrow{u_n}$, $\overrightarrow{v_n}$ and $\overrightarrow{e_z}$ also form a set of mutually orthogonal vectors, $\overrightarrow{v_n} = \overrightarrow{e_z} \times \overrightarrow{u_n},\ \forall n \in [1, N]$; i.e. in our case, the antenna radiates perpendicularly with respect to the robot's movement.
- $d_n,\ n \in [1, N]$: the distance between the tag and the n^{th} antenna location, $d_n = \|\boldsymbol{A}_{tag} - \boldsymbol{A}_n\|_2$.
- $\boldsymbol{A}_R$: the location among $\{\boldsymbol{A}_1, \cdots, \boldsymbol{A}_N\}$ used as reference point to craft distance differences. In the non straight case $\boldsymbol{A}_R$ represents the minimum antenna-to-tag distance.

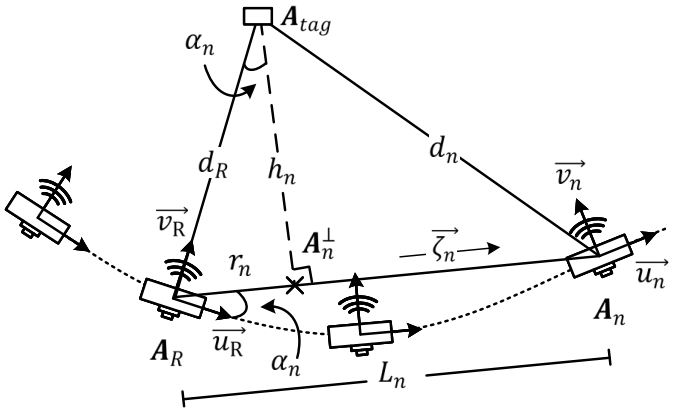

Fig. 6: Geometry of a non straight synthetic aperture.

Contextually, the phase measured at $\boldsymbol{A}_R$ is denoted as ϕ_R^{meas}.

- $\overrightarrow{u_R}$: the unit vector that represents the moving direction of the antenna at reference location $\boldsymbol{A}_R$. The line that joins the tag with the reference location is considered perpendicular to the direction of motion at reference location, $\overrightarrow{\boldsymbol{A}_R\boldsymbol{A}_{tag}} \perp \overrightarrow{u_R}$.
- $\overrightarrow{v_R}$: the unit vector that represents the direction of antenna's radiation at reference location $\boldsymbol{A}_R$. The line that joins the tag with the reference location is considered parallel to the direction of radiation at reference location, $\overrightarrow{\boldsymbol{A}_R\boldsymbol{A}_{tag}} \parallel \overrightarrow{v_R}$.
- d_R: the distance between the reference point and the tag, $d_R = \|\boldsymbol{A}_{tag} - \boldsymbol{A}_R\|_2$. It is considered the shortest distance between the tag and the trajectory of the antenna.
- $L_n,\ n \in [1, N] - \{R\}$: the distance between the reference and the n^{th} antenna location, $L_n = \|\boldsymbol{A}_R - \boldsymbol{A}_n\|_2$.
- $\overrightarrow{\zeta_n},\ n \in [1, N] - \{R\}$: the unit vector in the direction of the line that joins the reference point with the n^{th} location, $\overrightarrow{\zeta_n} = \overrightarrow{\boldsymbol{A}_R\boldsymbol{A}_n} = \dfrac{\boldsymbol{A}_n - \boldsymbol{A}_R}{\|\boldsymbol{A}_n - \boldsymbol{A}_R\|_2}$.
- $\alpha_n,\ n \in [1, N] - \{R\}$: the acute value of the angle between the direction of motion at reference point $\overrightarrow{u_R}$ and direction $\overrightarrow{\zeta_n}$, $\alpha_n = \arccos(\overrightarrow{u} \cdot \overrightarrow{\zeta_n})$. Moreover, the angle defined by points $\boldsymbol{A}_R$, $\boldsymbol{A}_{tag}$ and $\boldsymbol{A}_n$ is equal to α_n, since the sides of the former are perpendicular to the sides of the latter.
- $\boldsymbol{A}_n^{\perp},\ n \in [1, N] - \{R\}$: the point on the direction of $\overrightarrow{\zeta_n}$ with the minimum distance from the tag. The line that joins the tag with $\boldsymbol{A}_n^{\perp}$ is perpendicular to $\overrightarrow{\zeta_n}$. As a result, the formed triangles $\triangle \boldsymbol{A}_{tag}\boldsymbol{A}_n\boldsymbol{A}^{\perp}$ and $\triangle \boldsymbol{A}_{tag}\boldsymbol{A}_R\boldsymbol{A}^{\perp}$ are right.
- h_n: the altitude of triangle $\triangle \boldsymbol{A}_{tag}\boldsymbol{A}_n\boldsymbol{A}^R$ that is through vertex $\boldsymbol{A}_{tag}$ and perpendicular to the opposite side, $h_n = \|\boldsymbol{A}_{tag} - \boldsymbol{A}_n^{\perp}\|_2$
- r_n: the distance between reference point $\boldsymbol{A}_R$ and $\boldsymbol{A}_n^{\perp}$, $r_n = \|\boldsymbol{A}_R - \boldsymbol{A}_n^{\perp}\|_2$.

According to the above scheme, the tag's position is calculated by:

$$\boldsymbol{A}_{tag}^{2D} = \boldsymbol{A}_R + d_R\overrightarrow{v_R} \tag{16}$$

where the unknown variable that seeks estimation is now distance d_R. The distance between the n^{th} with $n \in [1, N] - \{R\}$ antenna location and the tag is:

$$d_n = \sqrt{(r_n \pm L_n)^2 + h_n^2}, \tag{i}$$

while the distance between the reference location and the tag is given by:

$$d_R = \sqrt{r_n^2 + h_n^2}, \tag{ii}$$

For the n^{th} antenna location, the difference between the aforementioned distances is defined as:

$$\begin{gathered}\Delta d_n = d_R - d_n \Rightarrow \\ \Delta d_n = \sqrt{r_n^2 + h_n^2} - \sqrt{(r_n \pm L_n)^2 + h_n^2}.\end{gathered} \tag{iii}$$

By raising (iii) to the square, the latter becomes

$$\begin{gathered}\Delta d_n^2 = r_n^2 + h_n^2 - 2\sqrt{r_n^2 + h_n^2}\sqrt{(r_n \pm L_n)^2 + h_n^2} + \\ +(r_n \pm L_n)^2 + h_n^2\end{gathered} \tag{iv}$$

By substituting (iii) into (iv):

$$\begin{gathered}\Delta d_n^2 = r_n^2 + h_n^2 - 2\sqrt{r_n^2 + h_n^2}(\sqrt{r_n^2 + h_n^2} - \Delta d_n) + \\ +(r_n \pm L_n)^2 + h_n^2 \Rightarrow \\ \Delta d_n^2 = 2\sqrt{r_n^2 + h_n^2}\Delta d_n \pm 2 r_n L_n + L_n^2.\end{gathered} \tag{v}$$

However, in each triangle $\triangle \boldsymbol{A}_{tag}\boldsymbol{A}_n\boldsymbol{A}^{\perp}$,

$$r_n = \sin(a_n) d_R, \quad n \in [1, N] - \{R\} \tag{vi}$$

and after substituting (ii) and (vi) in (v):

$$\Delta d_n^2 = 2 d_R \Delta d_n \pm 2 \sin(a_n) d_R L_n + L_n^2 \tag{vii}$$

Angle a_n is known, because the trace of the robot, along with its pose (position and orientation) are known. Eventually, by substituting (6) in (vi), an algebraic relation is formed, which associates the unknown quantity d_R with a known phase difference:

$$\left(\frac{\lambda}{4\pi}\Delta\breve{\phi}_n^{meas}\right)^2 - L_n^2 = 2\left(\frac{\lambda}{4\pi}\Delta\breve{\phi}_n^{meas} \pm \sin(a_n) L_n\right) d_R, \tag{17}$$

where $\Delta\breve{\phi}_n^{meas} = \breve{\phi}_R^{meas} - \breve{\phi}_n^{meas}$ is the difference between the unwrapped phase recorded at the reference location $\breve{\phi}_R^{meas}$ and the $n^{th},\ n \in [1, N] - \{R\}$ phase measurement $\breve{\phi}_n^{meas}$. The matrix form of the constructed linear system based on (17), is given by:

$$\boldsymbol{A}\boldsymbol{x} = \boldsymbol{b}$$

$$\boldsymbol{A} = 2\begin{bmatrix} \frac{\lambda}{4\pi}\Delta\breve{\phi}_1^{meas} \pm \sin(a_1) L_1 \\ \frac{\lambda}{4\pi}\Delta\breve{\phi}_2^{meas} \pm \sin(a_2) L_2 \\ \vdots \\ \frac{\lambda}{4\pi}\Delta\breve{\phi}_{N-1}^{meas} \pm \sin(a_N) L_{N-1} \end{bmatrix} \quad \boldsymbol{x} = \begin{bmatrix} d_R \end{bmatrix}$$

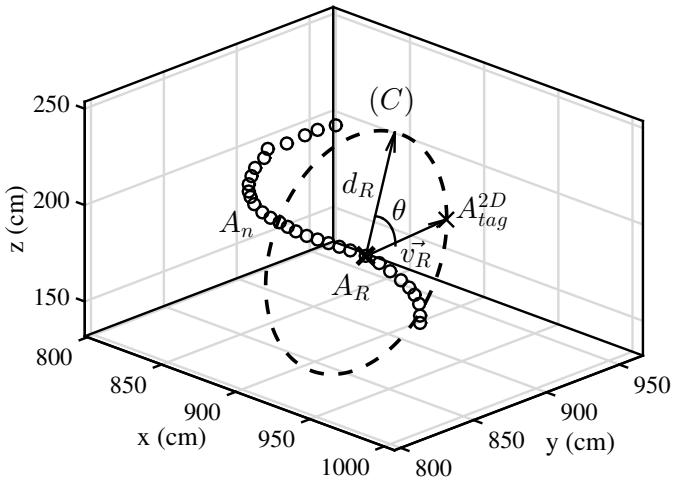

Fig. 7: The 3D locus of possible tag locations corresponding to a non straight synthetic aperture.

$$\boldsymbol{b} = \begin{bmatrix} \left(\frac{\lambda}{4\pi}\Delta\breve{\phi}_1^{meas}\right)^2 - (L_1)^2 \\ \left(\frac{\lambda}{4\pi}\Delta\breve{\phi}_2^{meas}\right)^2 - (L_2)^2 \\ \vdots \\ \left(\frac{\lambda}{4\pi}\Delta\breve{\phi}_{N-1}^{meas}\right)^2 - (L_{N-1})^2 \end{bmatrix} \tag{18}$$

System is again an overdetermined system of $N-1$ equations but with 1 unknown coefficient this time, $\boldsymbol{x} = [d_R]$. The solution is computed in a least-square sense (10) and eventually the tag's location is derived by (16).

Equation (16) solves the localization problem at the antenna's horizontal plane. The 3D interpretation of the solution though, is a circular locus lying in the plane parallel to $\overrightarrow{v_R}$ and $\overrightarrow{e_z}$ (with $\overrightarrow{u_R}$ being the normal vector), has center $\boldsymbol{A}_R$ and radius d_R, see Fig. 7. In Fig. 7, we assume that the robot always moves along the xy plane. The parametric equations of the above circle are given by:

$$\begin{cases} x = A_{R_x} + d_R\cos(\theta)v_{R_x} \\ y = A_{R_y} + d_R\cos(\theta)v_{R_y} \\ z = A_{R_z} + d_R\sin(\theta) \end{cases} \tag{19}$$

where A_{R_x}, A_{R_y}, A_{R_z} are the x, y, z coordinates of center point $\boldsymbol{A}_R$ respectively, v_{R_x} and v_{R_y} are the x and y components of vector $\overrightarrow{v_R}$, respectively and θ goes from 0 to π. By exploiting (19) any two coordinates of the tag can be calculated when one is known.

1) Reference Selection: In contrast to straight problems, where any antenna location $\boldsymbol{A}_n,\ n \in [1, N]$ could be used as reference, non straight cases demand for a specific selection. In particular, $\boldsymbol{A}_R$ should be the antenna location that represents the minimum antenna-to-tag distance and corresponds to the minimum value of the unwrapped phase $\breve{\phi}_n^{meas}$.

2) Evaluation: Similarly to III-A2, the confidence of the estimation is quantified by the variance/standard deviation of the problem's unique unknown parameter d_R. Equation (18) defines a single-variable system; therefore, the covariance matrix $\boldsymbol{C}$ is a scalar and the standard deviation of the tag's two-dimensional estimation is given by:

$$\sigma_{est} = \sqrt{\sigma_{d_R}^2} = \sqrt{C}, \tag{20}$$

where $\boldsymbol{C}$ is computed by (14).

IV. Three-dimensional Localization by Multi-Antenna Aperture

The method proposed in III solves the two-dimensional localization problem by exploiting a single antenna. The three-dimensional interpretation of the solution corresponds to a circular locus of potential tag locations. By employing multiple antennas on the moving robot, the solution can be then reduced to a single point.

More specifically, let $M \geq 2$ moving antennas each of which generates a synthetic aperture at different height. By treating the measurements from each aperture independently and solving (9) or (18) for each antenna, M loci defined by (11) or (19) are introduced. Tag's location is theoretically released on their common intersection. However, since each locus is computed with some error, practically the loci do not intersect in 3D space. Therefore, the intersection problem is treated in a least-square sense, according to which, the point with the the minimum distance from all created loci represents the estimated solution, as shown in Figs 8 (a) and (b).

Let the circle (C) of Fig. 9 , defined by center $\boldsymbol{A}$, radius R and normal vector $\overrightarrow{N}$. Let also a point $\boldsymbol{P}$ in 3D space and $\boldsymbol{P'}$ its projection to the circle's plane. The distance between points $\boldsymbol{P}$ and $\boldsymbol{K}$ represents the minimum distance between point $\boldsymbol{P}$ and circle (C). This distance is denoted as $D_{\boldsymbol{PC}}$ and computed by:

$$\begin{aligned} D_{\boldsymbol{PC}} &= \|\boldsymbol{P} - \boldsymbol{K}\| = \sqrt{\|\boldsymbol{P} - \boldsymbol{P'}\|^2 + \|\boldsymbol{P'} - \boldsymbol{K}\|^2} = \\ &= \sqrt{\left(\overrightarrow{N}\cdot(\boldsymbol{P} - \boldsymbol{A})\right)^2 + \left(\|\overrightarrow{N}\times(\boldsymbol{P} - \boldsymbol{A})\| - R\right)^2} \end{aligned} \tag{21}$$

Circle (C) of Fig. 21 essentially represents the circular locus derived by PD-Loc. Therefore in (21), $\boldsymbol{A} = \boldsymbol{A}^{\perp}$, $R = h$ and $\overrightarrow{N} = \overrightarrow{u}$ in case of a straight synthetic aperture (see Fig. 5), and $\boldsymbol{A} = \boldsymbol{A}_R$, $R = d_R$ and $\overrightarrow{N} = \overrightarrow{u_R}$ in the non straight case (see Fig. 7).

The point that minimizes the sum of squared distances from all calculated circular loci $(C_i),\ i \in [1, M]$ corresponds to the estimation of the tag's location in 3D space:

$$\boldsymbol{A}_{tag}^{3D} = \arg\min_{\boldsymbol{P}} \sum_{i}^{M} \left(w_i D_{\boldsymbol{PC}_i}\right)^2 \tag{22}$$

where (22) represents a weighted least square problem with $w_i,\ i \in [1, M]$ being the weight of the i^{th} locus. For $w_i = 1$, (22) will identify the point that minimizes its sum of distances from all loci. However, by properly sizing w_i, we can identify the solution to be closer to loci with greater "trust". Each locus (C_i) has been calculated by estimating the solution of a linear

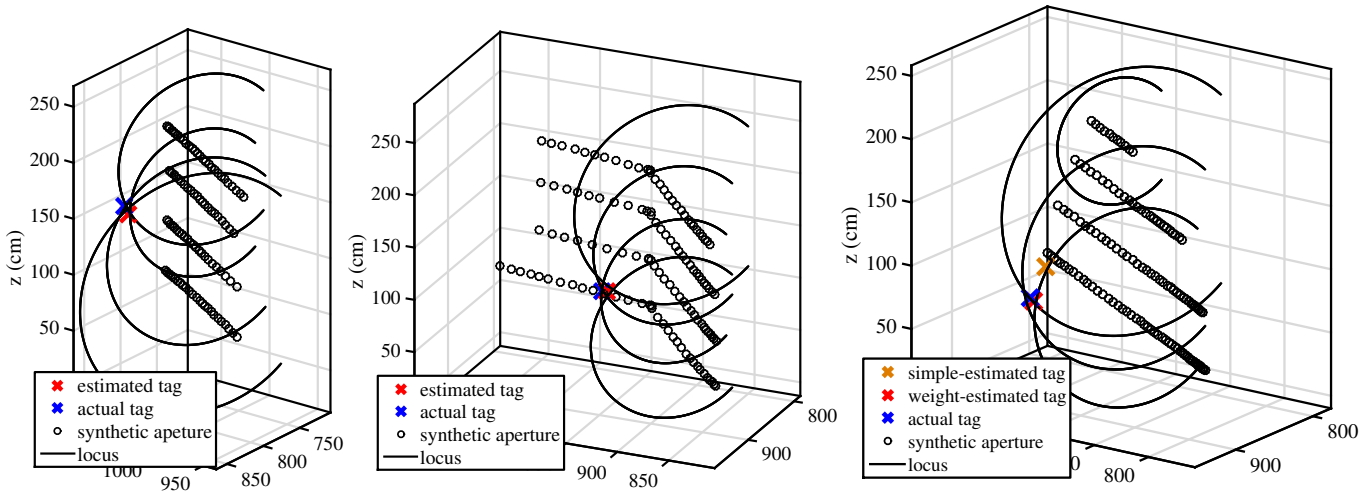

(a) Loci intersection in case of straight robot's path

(b) Loci intersection in case of non straight robot's path

(c) Confidence-based weights introduced in the loci-intersection problem improve the estimation.

Fig. 8: Solution of the 3D localization problem by multi-antenna aperture.

system and as a consequence, the reliability of each locus is expected to differ. Loci based on reliable estimations of the system's parameters should have a great impact to the solution and should be assigned with larger weights, whilst loci defined by poor estimations should contribute less. In this context, we propose to exploit the reciprocal of the variance, related to the estimated locus from each antenna, such that:

$$w_i = \left(\frac{1}{\sigma_{est_i}} \right), \quad i \in [1, M], \tag{23}$$

where σ_{est_i} represents the confidence of the i^{th} locus, quantified by the standard deviation of the corresponding two-dimensional tag estimation (15); the smaller the standard deviation of an estimation, the larger the assigned weight.

Fig. 8 (c) demonstrates the necessity of exploiting weights in (22). The upper antenna collected an unsatisfactory amount of measurements and led to a poor estimation of the tag's locus. The antenna's locus is situated too far from the other three loci, which were derived by data with better "quality" (smaller variance in the estimation). When each circle contributes the same in (22), the unreliable locus "pulls" the estimated solution away from the actual. On the contrary, weighted least square is able to neglect the upper circle and identify a solution that is close to the other three circles.

V. Simulative Results

Monte Carlo simulations were conducted to evaluate the effectiveness of the method's variations in III-A and III-B and discover their strengths and weaknesses at treating the two dimensional localization problem by a single antenna. Two types of antenna trajectories were simulated and Fig. 10 depicts the resulted synthetic apertures: i) a straight and ii) a non straight of "U"-type. The variables that were investigated throughout the simulative analysis are the distance d between the aperture and the simulated tag and the sampling interval

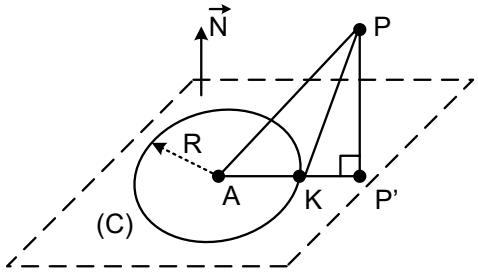

Fig. 9: Minimum distance between a point P and a circle (C).

of the aperture Δs; i.e. the distance the antenna travelled between two successive measurements of the tag. A uniform sampling has been considered. Each aperture is determined by a fixed length of 3m and the considered sampling interval essentially defines the number of available phase measurements for processing. For instance, an interval of 2 cm indicates that the simulated antenna collects one measurement every 2 cm of spatial displacement, resulting in 150 measured samples for a total travelled distance of 3 m. For each pair of distance's and sampling interval's values, 50000 tag positions were randomly generated at different locations to evaluate the method's performance.

The unwrapped phase model used through the numerical analysis is:

$$\breve{\phi}_n^{sim} = \breve{\phi}_n^{exp} + \phi_n^{noise}, \ n \in [1, N] \tag{24}$$

where $\breve{\phi}_n^{exp}$ represents the unwrapped phase of the direct (LOS) field ray, which is given by (5) for $\phi_0 = 0$, while ϕ_n^{noise} accounts for zero-mean Gaussian noise with standard deviation 0.1 rads.

Fig. 11 demonstrates the main difference between the expected performance of a straight and a non straight trajectory. In general, PD-Loc can be discriminated in two parts. The first one corresponds to the computation of a line that the tag may

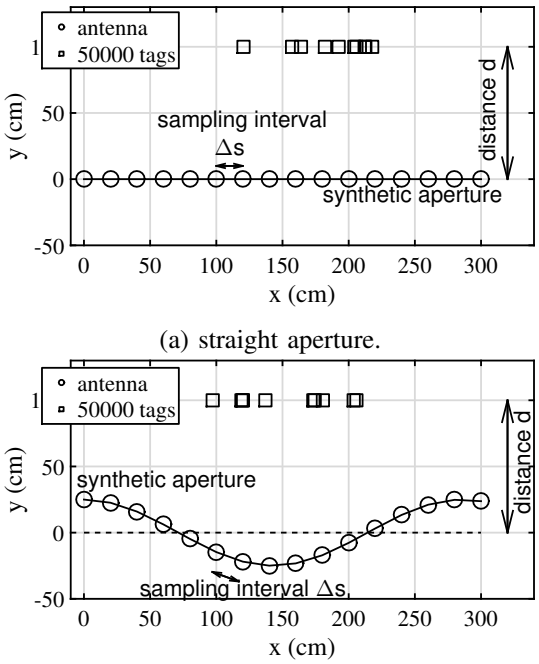

(a) straight aperture.

(b) non straight aperture.

Fig. 10: The simulated configurations. The sampling interval of the apertures and the tag-to-aperture distance represent the variables of the simulations.

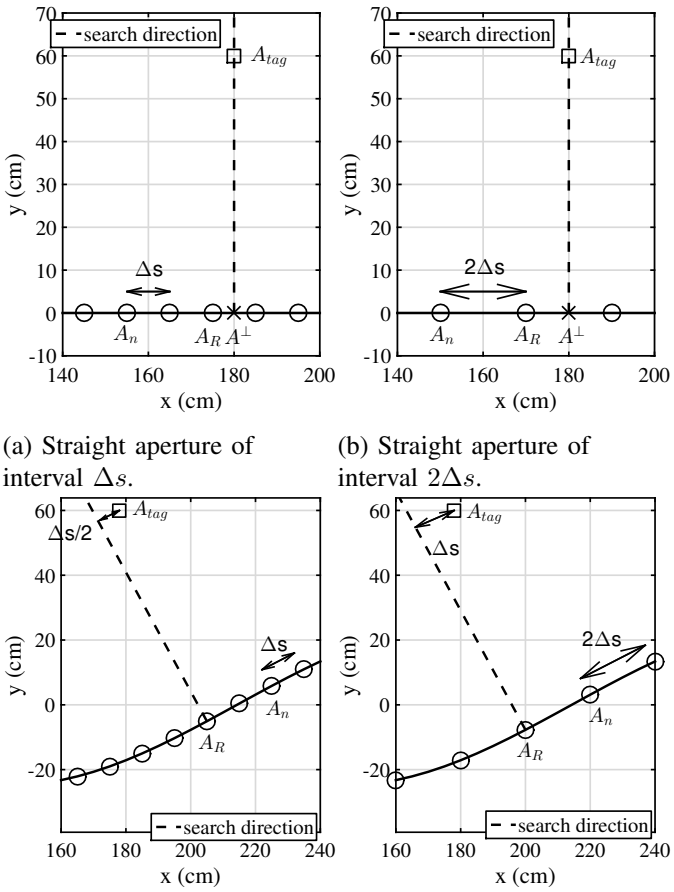

(a) Straight aperture of interval Δs.

(b) Straight aperture of interval $2\Delta s$.

(c) Non straight aperture of interval Δs.

(d) Non straight aperture of interval $2\Delta s$.

Fig. 11: Performance investigation for different types of apertures.

be located, while the second part represents the computation of the tag's range along that line. Due to the geometry of a straight problem, the corresponding system (9) is capable of treating both parts. By estimating parameter r, a point $\boldsymbol{A}^\perp$ is found that is not necessarily a point at which the antenna recorded a measurement. The tag may be located on the line that goes through $\boldsymbol{A}^\perp$ and is perpendicular to the direction of the antenna's motion. By computing d_R, the tag's range along that line is estimated. On the contrary, system (18) of the non straight problem is capable of estimating only one parameter, which is the tag's distance along a given line. In a dissimilar way to straight cases, point $\boldsymbol{A}^\perp$ that determines the line the tag may be located on, is not computed but selected among the locations at which the antenna recorded a measurement. This point is also used as reference $\boldsymbol{A}_R$.

As a direct consequence of the above, the sampling interval Δs of a straight antenna array is not expected to affect the accuracy of the method. No matter how sparse the antenna locations are, a point $\boldsymbol{A}^\perp$ could be always estimated in between to define the perpendicular line the tag may be situated; see Fig. 11 (a) and (b), where that line represents the search direction of the tag. On the other hand, sampling interval will play an important role in non straight cases, since that line has to pass necessarily through an aperture's location and more specifically, reference location $\boldsymbol{A}_R$. The sparser the aperture is, the more the search direction can miss the actual tag's position, as demonstrated in Fig. 11 (c) and (d).

The findings of the investigation are presented in Fig. 12, where the average localization error (of 50000 randomly simulated tags) for increasing values of sampling interval and tag-to-antenna distance is presented. Fig. 12 (a) corresponds to the straight simulated aperture shown in Fig. 10 (a). The achieved error is quite low, while the performance remains unaffected by increasing either the sampling interval or the distance of the tag. This effect is expected, since the search direction of the tag, goes through the computed point $\boldsymbol{A}^\perp$, which can be anywhere along the antenna's path line, see Fig. 11 (a) and (b). As a result, the method's performance is independent of the distance between successive locations of the aperture. For instance, a tag placed 1m from the antenna's trajectory has been localized with a mean error of around 0.6 cm for any value of Δs. Similar behavior is met for any tag distance and aperture sampling.

Fig. 12 (b) demonstrates the localization error when the non straight trajectory of Fig. 10 (b) is employed. In this case, the achieved error mainly depends on Δs. For instance, a tag placed at 1 m distance from the synthetic aperture, has been localized with a mean error of 6 cm for $\Delta s = 0.1$cm, 8 cm for $\Delta s = 4$cm, 10 cm for $\Delta s = 10$cm for and 12 cm for $\Delta s = 14$cm, whilst the respective error achieved by the straight aperture was consistent (0.6 cm) for every deployed Δs. Furthermore, the further the tag is placed the higher the recorded localization error.

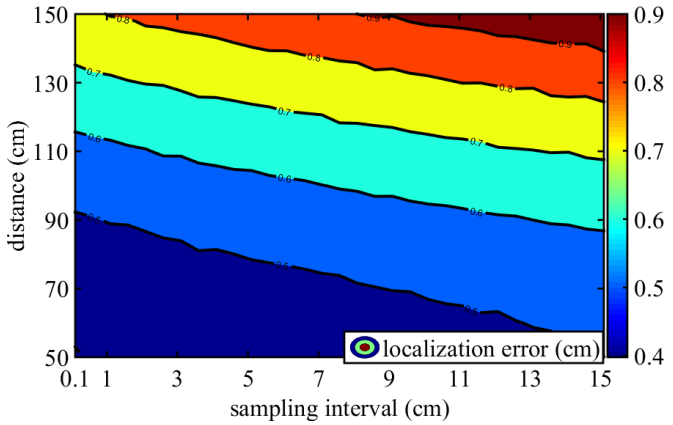

(a) straight aperture

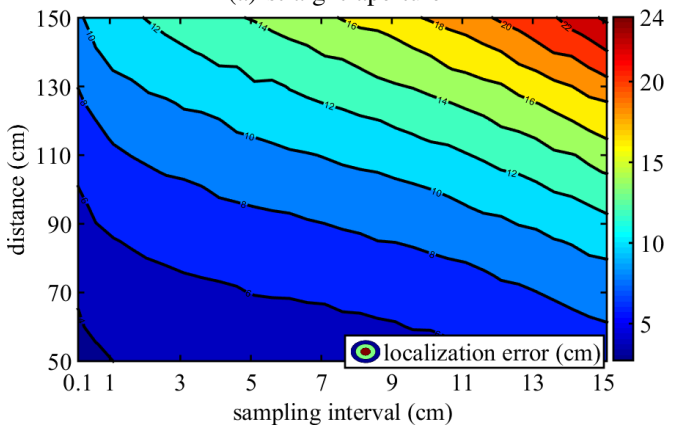

(b) non straight aperture

Fig. 12: Localization error with respect to the tag-to-aperture distance and the aperture's resolution.

Straight trajectories outperform non straight ones, even for cases where quite dense sampling is applied. For the densest sampling interval of $\Delta s = 0.1$cm, the straight aperture estimates a tag placed at the shortest distance ($d = 0.5$m) with a mean error of 0.4 cm, whilst the non straight aperture with a mean error of 4 cm; ten times worse. This indicates that non straight apertures require excessively dense sampling in order to accomplish similar performances with straight ones, a fact which may not be feasible in realistic applications, where the sampling rate is non-uniform and dependent of many factors (e.g. speed of robot, tag population in sight).

VI. Experiments

An experimental campaign took place in a School's laboratory room, employing the mobile robot of Fig. 13. The robot is equipped with the ROBOTNIK RB-1 mobile base and carries one 2D LIght Detection And Ranging (LIDAR) sensor, through which, it creates a 2D map of the environment and localise itself in it. It also carries one frontal and two lateral RGBD sensors for the purpose of creating a 3D map of the environment. As for the RFID equipment attached, the robot carries two RFID readers, and eight (four per side) laterally mounted antennas at the heights of 0.65m, 1.05m, 1.45m and 1.95m, respectively. Finally, a small form factor on-board

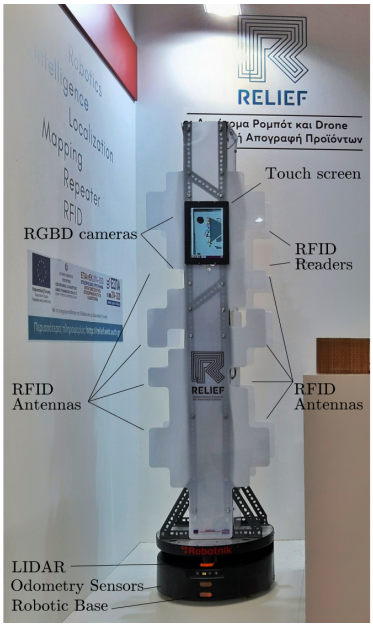

Fig. 13: Photo of robot "Frida" from a recent international exhibition.

(a) Two banners placed side-by-side

(b) Two banners placed back-to-back

Fig. 14: Photos during the experiments.

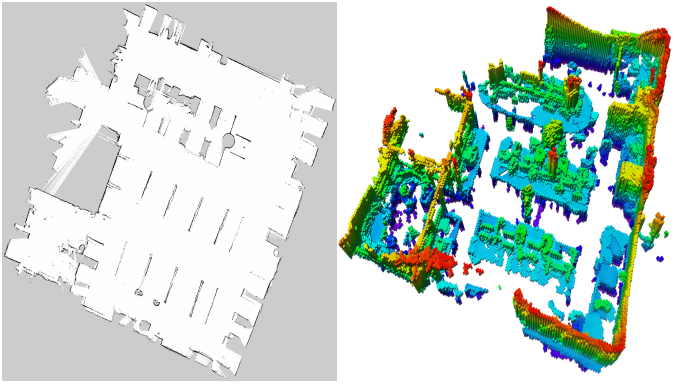

(a) 2D map

(b) 3D map

Fig. 15: The maps of the laboratory room created by "Frida" during an experiment.

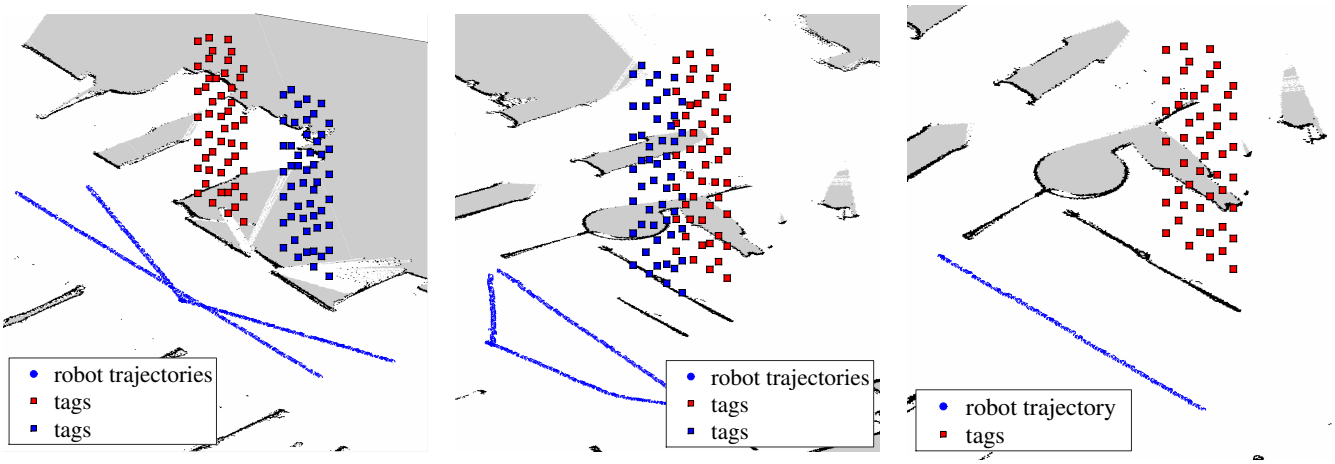

(a) Two banners placed side-by-side (b) Two banners placed back-to-back (b) Single banner

Fig. 16: Tag configurations and estimated robot trajectories of the conducted experiments, pinpointed in the environment's map.

computer is also employed to concentrate the measurements by the various sensors and process them online. 100 passive UHF RFID tags were mounted on two banners on a millimeter paper and the banners were set in various configurations to evaluate different tag populations and propagation conditions, as shown in Fig. 14.

The robot navigates in the vicinity of the RFID tags in various trajectories, while the RFID reader records the phase and power of the tags' backscattered signals. As the robot moves, it continuously tracks its own pose (x,y,θ) over time; this information is exploited to extract each antenna's coordinates and direction of motion. The existence of a map (Fig. 15) is a prerequisite for robot localisation. A map is derived by the continuous integration and matching of successive LIDAR or RGBD measurements, usually considering an estimate of the robot's motion between two measurements, which is extracted via odometry, while robot localization rests on the alignment of LIDAR measurements to the map of the environment in which the robot moves by considering the robot's motion model. In this specific implementation, mapping was performed via the "karto" SLAM algorithm [29], and estimation of the robot's trajectory was carried out through a modified version of the "amcl" algorithm [30].

The measurements were repeated five times, each of which corresponds to a different banner configuration and type of employed robot trajectory. Fig. 16 depicts the tags' locations and the estimated robot trajectories inside the created 2D map, during each of the five conducted experiments.

RFID-localization rests on the integration of the tag's measurements acquired by the reader's antennas, and the antennas' coordinates at each measurement, which are made available by the robot-localization algorithm. However, the locations of the antennas are estimated by processing noisy sensor and odometry data and thus, are expected to suffer from errors depending on the amcl algorithm's accuracy. Such errors will propagate to the tag estimations as well, affecting the accuracy of any method applied on such data.

A. Experimental Results of 2D localization

In this section, the problem of 2D localization by a single antenna (see section III) is evaluated and the respective results are presented. The tag's height is considered known, so the problem is reduced to the estimation of the x and y coordinates.

1) Confidence Evaluation: The RFID tags are attached on the banner at a minimum height of 0.1m and a maximum of 2.1m. Depending on their height, they will be illuminated and read by a different number of robot's antennas. For instance, tags placed at the banner's center ensure sufficient coverage by all four antennas, whilst tags attached at the bottom or top will be sufficiently read only by the antennas mounted at a similar height of the robot. The method is applied to estimate the location of a tag, despite the availability of its measurements; if a tag is read by four antennas, the method is applied independently to each of the four sets of measurements resulting in four different estimations for the same tag. Localization is performed even for cases where a small number of measurements is collected. Estimations based on such inadequate data will suffer from large localization error and consequently, deteriorate the method's accuracy. However, by exploiting the confidence metric introduced in section III, such estimation is possible to be identified and discarded. More specifically, the standard deviation of each estimation σ_{est}, calculated by (15) or (20), is examined and in case it exceeds a predefined threshold, the corresponding estimation is rejected. Recalling from section III, small values of σ_{est} indicate stronger reliability.

Fig. 17 plots the mean and the standard deviation of the achieved localization error for various values of desired confidence. Fig. 17 (a) corresponds to the results of the three experiments that employed a straight synthetic aperture, i.e. the robot moved along a straight path while collecting data and Fig. 17 (b) to the results of the two experiments, which employed non straight trajectories. Initially, no confidence-constraint is applied and the reported accuracy is quite low,

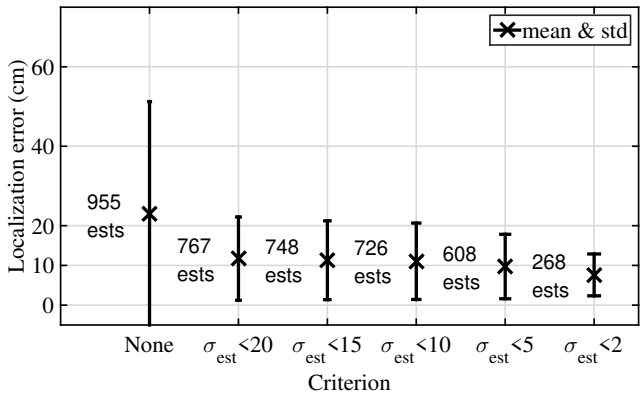

(a) Straight robot's trajectory

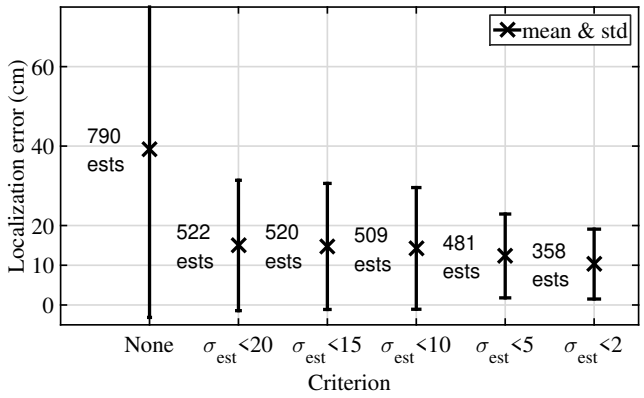

(b) Non straight robot's trajectory

Fig. 17: Error of two-dimensional localization when different confidence-thresholds are applied to reject poor estimations.

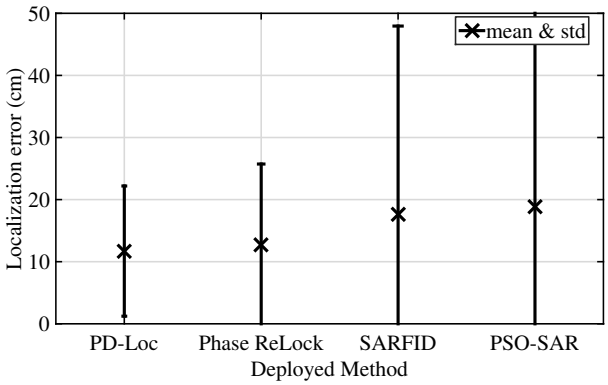

(a) Straight robot's trajectory

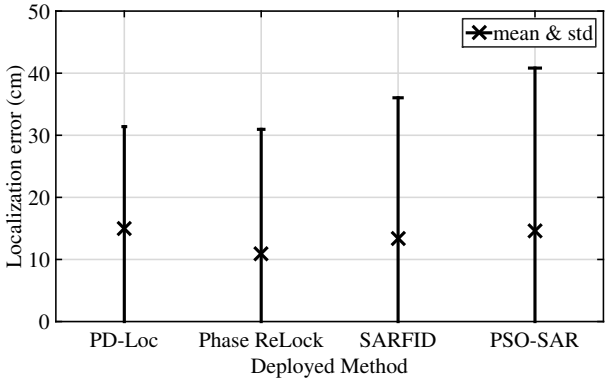

(b) Non straight robot's trajectory

Fig. 18: Error of two-dimensional localization achieved by each applied method.

since estimations based on inadequate measurements are included. Especially the standard deviation of the error is quite high, indicating the existence of estimations with significantly increased error. However, when reliability is taken into account, poor estimations are identified and excluded, leading to the improvement of the delivered accuracy. Even with the most relaxed constraint ($\sigma_{est} < 20$cm), the localization error decreases in the order of tens of cm compared to its initial value. The stricter the desired constraint becomes, the more the achieved error decreases at an expense of less accepted estimations. This effect verifies the functionality of the variance-based metric developed for both types of synthetic apertures.

As the findings of simulation-analysis in section V predicted, the localization accuracy delivered by a straight path is slightly better compared to a non straight path. For example, in case of rejecting estimations with $\sigma_{est} \geq 15$cm, the straight synthetic aperture is more accurate by 5cm compared to the non straight one.

2) PD-Loc vs prior art: Next, the method's performance is compared against prior art. Additionally to PD-Loc, three other SAR-based methods have been implemented and tested in the same experimental dataset to ensure fairness. The common feature the selected methods share is the Maximum Likelihood Estimation (MLE), according to which, the tag's estimated position should coincide with the global solution of a constructed objective function. Depending on the technique that global solution is sought, three approaches are identified:

a. Nonlinear Optimization (Phase ReLock [18]): The raw phase measurements collected along the aperture are initially unwrapped and in combination with a nonlinear phase-distance model, they represent the input to a data-fit problem. where the model's coefficients account for the tag's unknown coordinates in a 2D plane. The problem is solved in a least-square sense, while its convex-type property preserved by phase-unwrapping, allows rapid convergence to the problem's unique minimum through nonlinear optimization. This effect supports the real-time application of Phase ReLock.
b. Exhaustive Search over a grid (SARFID [14]): In this case, the matching function is non convex and suffers from multiple local minima and maxima. In order to identify the global solution, an exhaustive search is performed on a grid of potential tag locations assigned on the search-space. The grid point that maximizes a matching function corresponds to the estimated tag location. The required computations are proportional to the amount of candidate points and hence the execution time is increased; although a dense grid-resolution is expected to increase the method's accuracy. As a result, for dense and large grids, the real-time application of the method is not supported. In this specific experimental implementation , the exhaustive search was performed over

a grid extended to an area of of $4m \times 6m$ with a spacing value of 1 cm.

c. Particle Swarm Optimization (PSO-SAR [23]): The non convex cost function in [14] can be alternatively solved by particle swarm optimization. According to it, a swarm of particles that represent possible tag locations, is randomly generated within the search bounds and moving around the search space, seeking to identify the global solution. Each particle's evolution is affected by its own and its neighbors' best recorded locations. Although this method improves the computational cost of a grid-search, the accuracy and speed are still dependent of the algorithm's design parameters, e.g. the size of the particle swarm, each particle's initial location assigned. In this specific experimental implementation, a swarm of 100 particles was employed within the bounds of a $4m \times 6m$ search space.

The methods were applied only to tags that were estimated by PD-Loc with $\sigma_{est} < 15$cm to ensure fairness in the comparisons, since a sufficient collection of measurements is expected to be available for those tags.

The findings of our investigations are presented in Fig. 18. In case of a straight synthetic aperture, PD-Loc outperforms its competitors. It accomplished to locate the tags with a mean error of 10 cm and a std of 11 cm, while Phase ReLock delivered mean accuracy of 13 cm and std of 13 cm, PSO-SAR mean error 18 cm and std 30 cm and SARFID mean error 19 cm and std 35 cm. In case of the non straight paths though, PD-Loc features a slight increase of the achieved error, whilst the other three methods not. In general, SAR-based methods produce more reliable and accurate estimations when the synthetic aperture has component in two directions (the antenna moves in non straight trajectory), a property, which is not applicable in PD-Loc since the latter mainly depends on the geometry of the problem. Therefore, those methods are more accurate in comparison to their previous results regarding the straight paths. More particular, Phase ReLock reported the best accuracy (mean 11 cm and std 20 cm), PD-Loc delivered a mean error of 15 cm with 16 cm std, SARFID a mean error of 13 cm and a std 22 cm and finally PSO-SAR reported a mean 14 cm and a std 26 cm.

The authors here define the method as **"real-time"**, because **the collection of the measurements takes more time than the derivation of the estimations**. This is the case for both "PD-Loc" and "Phase Relock". During the movement of the robot, as soon as some data have been collected, (e.g. after 60s), PD-Loc is initiated, while the robot's readers continue to collect measurements; PD-Loc derives the estimations long before the robot requests new estimations with the updated measurements. Therefore, there is no queue (no buffering) whenever the localization method is invoked.

On the contrary, SARFID required about 1.8hour to perform the same amount of estimations, while PSO-SAR 0.8hours. It is worth noting that the estimation time of the latter methods depends on the size of grid and particle swarm deployed in this specific implementation and for denser grids and more particles, this time will be further increased. On the contrary, the speed of PD-Loc is stable, since it does not depend on any algorithm's design parameters.

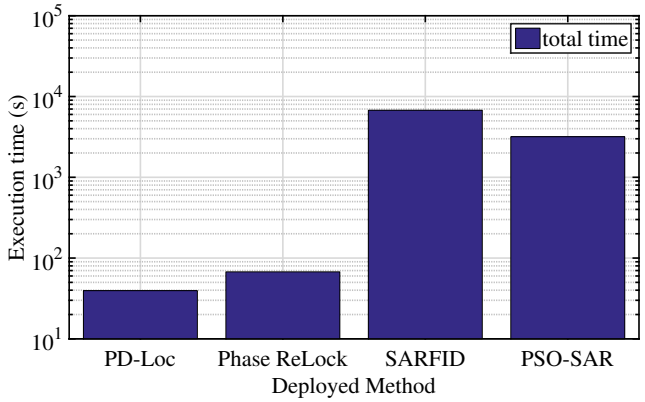

Fig. 19: Execution time required by each applied method for two-dimensional localization.

B. Experimental Results of 3D Localization

In this section the problem of 3D localization by multiple antennas (see section IV) is evaluated. During an experiment, each tag is interrogated by a maximum of four antennas. PD-Loc solves a linear system for each antenna independently and estimates a 3D locus around its trajectory, where the tag may be located; eventually it solves a least square problem to compute the location with the smallest distance from the loci.

1) PD-Loc vs prior art: Fig. 20 exhibits the localization error of PD-Loc compared to the three dimensional versions of the SAR-based methods of section VI-A2:

a. Nonlinear Optimization (Phase ReLock [21]): exploits a multi-antenna synthetic aperture and an unwrapped model to solve a multivariable convex-type optimization problem.

b. Exhaustive search over a grid (SARFID [22]): Similarly to the two-dimensional problem, SARFID seeks for the global maximum through exhaustive search over an assigned 3D grid of possible tag locations. In this specific experimental implementation, the search space is defined as an area of $4m \times 6m \times 2m$ with a grid resolution of 5 cm.

c. Particle Swarm Optimization (PSO-SAR [23]): The exhaustive search of [22] is replaced by a swarm of particles that move along the 3D space of interest to identify the global solution of the problem. In this specific experimental implementation, a swarm of 2000 particles was employed within the bounds of the $4m \times 6m \times 2m$ search space. Since the space of interest extends now in three dimensions, a greater number of particles is required in comparison to the 2D search-space.

Initially, PD-Loc solved the loci-intersection problem without accounting for the confidence of each locus, i.e. no weights were assigned to the least square problem of (22). In such case, the achieved localization error is about 45 cm for both straight and non straight path. However, the introduction of confidence-based weights improved the accuracy by decreasing the accomplished mean error to half (17 cm for straight apertures and 23 cm for non straight), verifying again experimentally the necessity of computing and exploiting the estimations' reliability. In case of straight aperture, PD-Loc outperformed its SAR-based competitors. In case of non straight aperture,

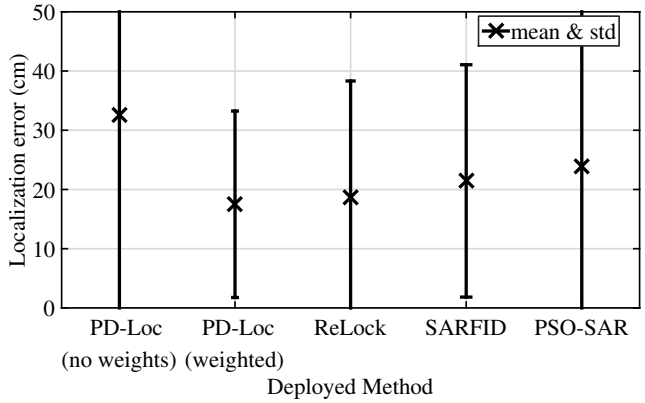

(a) straight robot's trajectory

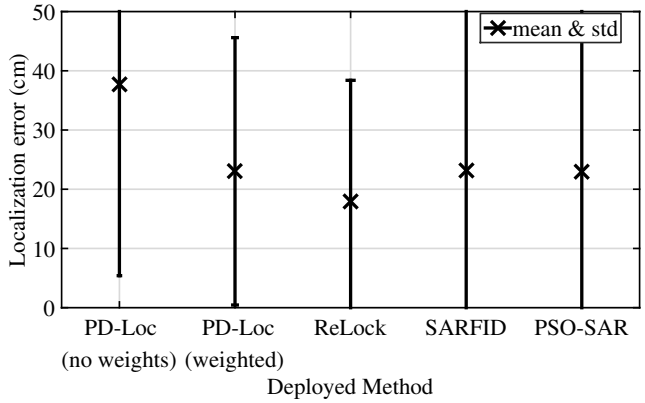

(b) non straight robot's trajectory

Fig. 20: Error of three-dimensional localization achieved by each applied method.

only Phase ReLock managed to deliver better performance (5 cm lower).

Last but not least, Fig. 21 compares the execution time of each method for all experiments (straight and non straight trajectories). The computational cost of the 3D extension of PD-Loc refers to the cost of unwrapping the phase measurements by each antenna, solving a linear least square problem for each antenna and solving the non linear least square problem of the loci-intersection. The cost of Phase ReLock refers to the cost of unwrapping the phase measurements by each antenna and solving a multi-antenna nonlinear optimization problem. The cost of SARFID refers to the cost of evaluating a matching function for an amount of grid-points and finally the cost of PSO-SAR refers to the cost of updating the swarm of particles in a three-dimensional search space. Again, PD-Loc outperformed all methods and achieved to estimate 450 tags in only 55s, while Phase ReLock "finished" second in 75s. The time consuming search of SARFID in 3D-grid required much more time, nearly 5h, while processing a large number of particles delayed PSO-SAR, which executed in 4.5h.

C. Source of error

The proposed localization system deals with the actual problem, according to which its task is to localize both the robot's poses and the surrounding RFID tags. Therefore, the

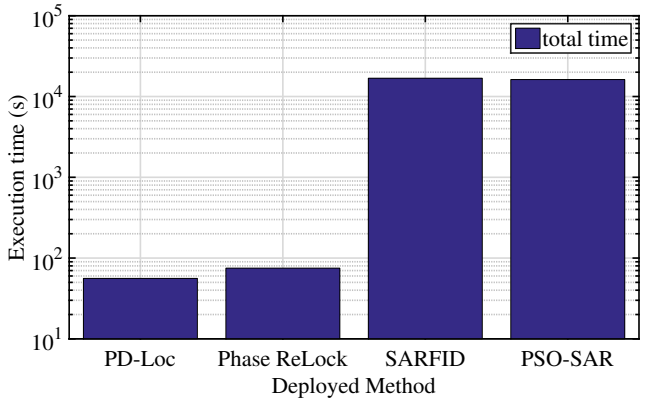

Fig. 21: Execution time required by each applied method for three-dimensional localization.

presented experimental accuracy is affected by various error sources.

The phase recorded by the RFID reader is essentially the phase of the resultant signal generated by the direct propagation ray (Line of Sight) and the rays from the various scatterers and reflectors (multipath). Since the presented localization algorithm exploits the free-space phase model (2), which does not account for multipath contributions, such mismatch between the actual and modeled phase is expected to introduce a localization error. Phase is also subjected to the effect of thermal noise and contains a random error that follows a typical Gaussian distribution [13], with a standard deviation of 0.1 radians.

Additionally, SAR-based localization algorithms require some sort of the antenna's position. In the proposed system, the antennas are mounted on a SLAM-enabled robot, which is capable of constructing a map of the environment and estimate its pose in it. However, such estimation is erroneous since it is based on noisy sensor data, while disformations of the produced map also influence the accuracy of the robot self-localization. Such errors propagate to the localization error of the RFID tags.

Finally, the tag locations on the banners have been measured with respect to a local coordinate system, the millimeter paper's system. The tag locations estimated by any RFID method applied refer to the map's coordinate system. These two systems should coincide in order to be able to evaluate the method's accuracy. Therefore, the locations of the banners inside the map are pinpointed and the local coordinate system of the banner is transformed to the map's system. This is a manual process and it is expected to introduce error in the influence the delivered accuracy.

VII. Conclusion

In this paper, we propose "PD-Loc", a novel SAR-based localization method that properly exploits phase differences and spatial properties of the problem's geometry to construct a linear overdetermined system. The solution of the system pinpoints the location of the tag. Thanks to the linearity of the problem, the system is solved rapidly by simple matrix operations. By properly exploiting the system's covariance matrix,

computed for the estimated parameter-values, the reliability of the tag's extracted location is quantified. This metric is then used to weight the importance of each synthetic aperture when 3D localization is sought by multiple antennas.

Initially, the problem is solved in 2D-space for straight and non-straight robot's trajectories. Simulations showed that the non-straight trajectories are vulnerable to larger errors as the aperture's sampling interval increases, because, for non-straight paths, the method is sensitive to the sampling point, where the minimum unwrapped phase was recorded; a finding which was also experimentally verified.

By extending the solution in 3D-space, circular loci of possible tag locations around each antenna's aperture are derived. We identify the 3D location of the tag to be the point that minimizes its weighted Euclidean distance by all loci. The weights are assigned on each sythetic aperture, based on the variance-reliability metric related to the collected measurements by each antenna.

Experimental results and comparisons against state-of-the-art methods evaluate the system's efficiency. PD-Loc delivers best performance when straight antenna trajectories are deployed (11 cm error in 2D localization and 17 cm in 3D) and slightly reduced (but still better than other methods) when the antenna moves along non straight paths (15 cm error in 2D localization and 23 cm in 3D). Most importantly though, such accuracy has been accompanied by the smallest estimation-time. Thanks to the linearity of the crafted system, real-time applicability of the proposed method is feasible.

REFERENCES

[1] S. Siachalou, A. Bletsas, J. N. Sahalos and A. G. Dimitriou, "RSSI-based Maximum Likelihood Localization of Passive RFID Tags Using a Mobile Cart," *IEEE Wireless Power Transfer Conference (WPTC)*, Aveiro, Portugal, 2016.

[2] S. Subedi, E. Pauls, and Y. D. Zhang, "Accurate Localization and Tracking of a Passive RFID Reader based on RSSI Measurements," *IEEE Journal of Radio Frequency Identification*, vol. 1, no. 2, pp. 144-54, 2017.

[3] J. Zhang, Y. Lyu, J. Patton, S.C. G. Periaswamy, and T. Roppel, "BFVP: A Probabilistic UHF RFID Tag Localization Algorithm Using Bayesian Filter and a Variable Power RFID Model," *IEEE Transactions on Industrial Electronics*, vol. 65, no. 10, pp. 8250-8259, 2018.

[4] P. V. Nikitin, R. Martinez, S. Ramamurthy, H. Leland, G. Spiess, and K. V. S. Rao, "Phase Based Spatial Identification of UHF RFID Tags," *2010 IEEE International Conference on RFID*, Orlando, Florida, 2010.

[5] J. Zhou, H. Zhang, and L. Mo, "Two-dimension Localization of Passive RFID Tags Using AOA Estimation," *2011 IEEE Instrumentation and Measurement Technology Conference (I2MTC)*, Binjiang, China, 2011.

[6] S. Azzouzi, M. Cremer, U. Dettmar, R. Kronberger, and T. Knie, "New Measurement Results for the Localization of UHF RFID Transponders Using an Angle of Arrival (AoA) Approach," *2011 IEEE International Conference on RFID*, Orlando (Fl), 2011.

[7] S. Subedi, E. Pauls, and Y. D. Zhang, "Accurate Localization and Tracking of a Passive RFID Reader based on RSSI Measurements," *IEEE Journal of Radio Frequency Identification*, vol. 1, no. 2, pp. 144-54, 2017.

[8] T. Liu, L. Yang, Q. Lin, Y. Guo, and Y. Liu, "Anchor-free backscatter positioning for RFID tags with high accuracy," *IEEE INFOCOM*, 2014, pp. 379—387.

[9] O. Frey, C. Magnard, M. Ruegg, and E. Meier, "Focusing of airborne synthetic aperture radar data from highly nonlinear flight tracks," *IEEE Trans. Geosci. Remote Sens.*, vol. 47, no. 6, pp. 1844–1858, Jun. 2009.

[10] R. Miesen, F. Kirsch, and M. Vossiek, "UHF RFID localization based on synthetic apertures," *IEEE Transactions on Automation Science and Engineering*, vol. 10, no. 3, pp. 807-815, 2013.

[11] A. Parr, R. Miesen and M. Vossiek, "Inverse SAR approach for localization of moving RFID tags," *2013 IEEE International Conference on RFID (RFID)*, 2013, pp. 104-109, doi: 10.1109/RFID.2013.6548142.

[12] A. Buffi, P. Nepa and F. Lombardini, "A Phase-Based Technique for Localization of UHF-RFID Tags Moving on a Conveyor Belt: Performance Analysis and Test-Case Measurements," in *IEEE Sensors Journal*, vol. 15, no. 1, pp. 387-396, Jan. 2015, doi: 10.1109/JSEN.2014.2344713

[13] L. Yang, Y. Chen, X.-Y. Li, C. Xiao, M. Li, and Y. Liu, "Tagoram: real-time tracking of mobile rfid tags to high precision using cots devices," *In Proceedings of the 20th annual international conference on Mobile computing and networking*, pp. 237-248, 2014.

[14] A. Motroni et al., "SAR-Based Indoor Localization of UHF-RFID Tags via Mobile Robot," *2018 International Conference on Indoor Positioning and Indoor Navigation (IPIN)*, 2018, pp. 1-8, doi: 10.1109/IPIN.2018.8533847.

[15] L. Shangguan and K. Jamieson, "The design and implementation of a mobile rfid tag sorting robot," *In Proceedings of the 14th Annual International Conference on Mobile Systems, Applications, and Services*, pp. 31-42, 2016.

[16] E. DiGiampaolo, F. Martinelli, "A Robotic System for Localization of Passive UHF-RFID Tagged Objects on Shelves," *IEEE Sensors Journal*, vol. 18, no. 20, pp. 8558–8568, 2018.

[17] E. DiGiampaolo and F. Martinelli, "A Passive UHF-RFID System for the Localization of an Indoor Autonomous Vehicle," *IEEE Transactions on Industrial Electronics*, vol. 59, no. 10, pp. 3961-3970, Oct. 2012, doi: 10.1109/TIE.2011.2173091.

[18] A. Tzitzis et al., "Localization of RFID Tags by a Moving Robot, via Phase Unwrapping and Non-Linear Optimization," in *IEEE Journal of Radio Frequency Identification*, vol. 3, no. 4, pp. 216-226, Dec. 2019, doi: 10.1109/JRFID.2019.2936969.

[19] E. Giannelos, E. Andrianakis, K. Skyvalakis, A. G. Dimitriou and A. Bletsas, "Robust RFID Localization in Multipath with Phase-Based Particle Filtering and a Mobile Robot," in *IEEE Journal of Radio Frequency Identification*, doi: 10.1109/JRFID.2021.3086759.

[20] A. Tzitzis et al., "Trajectory Planning of a Moving Robot Empowers 3D Localization of RFID Tags with a Single Antenna," in *IEEE Journal of Radio Frequency Identification*, doi: 10.1109/JRFID.2020.3000332.

[21] A. Tzitzis, A. Raptopoulos Chatzistefanou, T. V. Yioultsis and A. G. Dimitriou, "A Real-Time Multi-Antenna SAR-Based Method for 3D Localization of RFID Tags by a Moving Robot," in *IEEE Journal of Radio Frequency Identification*, vol. 5, no. 2, pp. 207-221, June 2021, doi: 10.1109/JRFID.2021.3070409.

[22] A. Motroni, P. Nepa, P. Tripicchio, M. Unetti, "A Multi-Antenna SAR-based method for UHF RFID Tag Localization via UGV", *2018 IEEE International Conference on RFID Technology & Application (RFID-TA)*, Macau, China, 2018.

[23] F. Bernardini et al., "Particle Swarm Optimization in SAR-Based Method Enabling Real-Time 3D Positioning of UHF-RFID Tags," in *IEEE Journal of Radio Frequency Identification*, vol. 4, no. 4, pp. 300-313, Dec. 2020, doi: 10.1109/JRFID.2020.3005351.

[24] A. Almaaitah, K. Ali, H. S. Hassanein, and M. Ibnkahla, "3D passive tag localization schemes for indoor RFID applications," *2010 IEEE International Conference on Communications*, pp. 1—5, 2010.

[25] F. Tlili, N. Hamdi, and A. Belghith, "Accurate 3D localization scheme based on active RFID tags for indoor environment," *IEEE RFID-TA*, 2012, pp. 378—382.

[26] Y. Zhang, L. Xie, Y. Bu, Y. Wang, J. Wu, and S. Lu, "3-Dimensional Localization via RFID Tag Array," *2017 IEEE 14th International Conference on Mobile Ad Hoc and Sensor Systems*, 2017

[27] L. Qiu, Z. Huang, N. Wirstrom, and T. Voigt, "3DinSAR: Object 3D Localization for Indoor RFID Applications," *IEEE International Conference on RFID (RFID)*, 2016.

[28] M. Gareis, P. Fenske, C. Carlowitz and M. Vossiek, "Particle Filter-Based SAR Approach and Trajectory Optimization for Real-Time 3D UHF-RFID Tag Localization," *2020 IEEE International Conference on RFID (RFID)*, 2020, pp. 1-8, doi: 10.1109/RFID49298.2020.9244917.

[29] K. Konolige, G. Grisetti, R. Kümmerle, W. Burgard, B. Limketkai and R. Vincent, "Efficient Sparse Pose Adjustment for 2D mapping," *2010 IEEE/RSJ International Conference on Intelligent Robots and Systems*, pp. 22-29, 2010, doi: 10.1109/IROS.2010.5649043.

[30] A. Filotheou, E. G. Tsardoulias, A. G. Dimitriou, A. L. Symeonidis and L. Petrou, "Pose selection and feedback methods in tandem combinations of particle filters with scan-matching for 2D mobile robot localisation," *J. Intell. Robot. Syst.*, vol. 100, pp. 925-944, 2020.

Anastasios Tzitzis was born in Thessaloniki, Greece, in 1994. In 2018 he received the Diploma in Electrical and Computer Engineering from Aristotle University of Thessaloniki, where he is currently working toward the Ph.D. degree. At the same time, he is working as a Research and Teaching Assistant at the Aristotle University. His current research interests include analysis and design of antennas, RFID technology, localization and wave propagation.

Andreana Malama was born in Kavala, Greece, in 1996. She received the Diploma in Electrical and Computer Engineering from the Aristotle University of Thessaloniki (AUTH) in 2020. She is currently involved in the research project "CultureID", where she investigates interactions between humans, robots and RFID-tagged exhibits inside the Archaeological Museum of Thessaloniki. Her main field of interest is Data Science.

Vasiliki Drakaki was born in Ierapetra, Greece in 1996. She received the MSc degree in Electrical and Computer Engineering from the Aristotle University of Thessaloniki, Department of Electrical and Computer Engineering in 2020. She is currently involved in the research project "CultureID", where she investigates interactions between humans, robots and RFID-tagged exhibits inside the Archaeological Museum of Thessaloniki. Her main interests are in the field of Data Analytics.

Aggelos Bletsas received the Diploma degree (with honors) in Electrical and Computer Engineering from Aristotle University of Thessaloniki, Greece in 1998, and the M.Sc. and Ph.D. degrees from MIT, Cambridge, MA, USA, in 2001 and 2005, respectively. He has worked at Mitsubishi Electric Research Laboratories (MERL), Cambridge, MA and RadioCommunications Laboratory (RCL), Department of Physics, Aristotle University of Thessaloniki. He currently serves as full Professor, School of Electrical & Computer Engineering, Technical University of Crete, Greece. His research interests span the broad area of scalable wireless communications and sensor networking, with emphasis on ultra-low power/cost environmental sensing, backscatter radio and ambiently-powered inference networks. His current focus and contributions are relevant to wireless, batteryless, backscatter sensors for precision agriculture that cost a few Euros, consume a few microWatts and can be read with commodity receivers and smartphones. He has served as Associate Editor of *IEEE Transactions on Wireless Communications* (2015-2021) and *IEEE Wireless Communications Letters* (from foundation in 2011-2016) and Technical Program Committee (TPC) member of major IEEE conferences. Dr. Bletsas was co-recipient of the *IEEE Communications Society 2008 Marconi Prize Paper Award in Wireless Communications*, and various Best Student Paper Awards e.g., in IEEE RFID-TA 2011, IEEE ICASSP 2015, IEEE RFID-TA 2017, MOCAST 2018. He has been included in the Highly-Cited Greek Scientists list. One of his papers is ranked 1st in Google Scholar *Classic Papers in Computer Networks & Wireless Communication*.

Traianos V. Yioultsis (M'09) received the Diploma and the Ph.D. degrees in electrical and computer engineering from the Aristotle University of Thessaloniki, Greece, in 1992 and 1998, respectively. From 2001 to 2002, he was a Post-Doctoral Research Associate with the Department of Electrical and Computer Engineering, University of Illinois at Urbana–Champaign. Since 2002, he has been with the Department of Electrical and Computer Engineering, Aristotle University of Thessaloniki, where he is currently a Professor. His current interests include the analysis and design of antennas and microwave circuits with fast computational techniques, and the modeling of complex wave propagation problems. He has also served as a member of the Editorial Board for IEEE Communications Letters and several international conferences.

Antonis G. Dimitriou (S'01-M06-SM'14) received the diploma and the Ph.D degree in Electrical and Computer Engineering from the Aristotle University of Thessaloniki, Greece, in 2001, and 2006 respectively. Since 2007, he is with the School of Electrical and Computer Engineering of AUTh, where he currently serves as a teaching and research faculty member.

He has participated in more than 20 research projects, 9 of which since 2007 as a principal investigator in the fields of Robotics, RFIDs, and Wireless Sensor Networks. He is currently the coordinator of projects "RELIEF" and "CultureID", where prototype SLAM-capable terrestrial robots and drones are designed and constructed to interact with RFID-tagged items. He was a Management Committee Member in the ICT COST Action IC301 "Wireless Power Transmission for Sustainable Electronics (WiPE)". He is the author or co-author of approximately 60 journal and conference papers.

Dr. Dimitriou was the recipient of the Ericsson Award of Excellence in Telecommunications in 2001 and co-recipient of the student-paper award in the 2011 IEEE RFID-TA conference. He received the "IEEE Wireless Communications Letters Exemplary Reviewer" award in 2012 and 2014. He is a Senior IEEE Member since February 2014. He also serves as Associate Editor of IEEE Journal of Radio Frequency Identification and TPC member for major international conferences.